AIAA JOURNAL
Vol. 30, No. 2, February 1992

Experimental Investigation of Normal-Shock/Turbulent-Boundary-Layer Interactions with and without Mass Removal

M. J. Morris,* M. Sajben,† and J. C. Kroutil‡
McDonnell Douglas Research Laboratories, St. Louis, Missouri 63166

Interactions of a normal shock with a turbulent boundary layer over a flat surface were investigated with and without imposing mass removal. The approach flow was very nearly two-dimensional, with a uniform freestream Mach number of 1.48, strong enough to cause separation at the shock foot. Suction was imposed immediately upstream of the shock over a finely perforated surface, removing much of the boundary-layer flow. The time-mean wall pressure distributions and two components of the time-mean velocity vector field were determined for both cases. Mass removal distorted the original shock pattern and eliminated the separation at the shock foot while reducing the boundary-layer thicknesses and growth rates to less than half. Mass removal also introduced some undesirable effects: asymmetric sidewall boundary-layer growth in the subsonic flow and increased shock oscillation amplitudes. The removed mass flow varied strongly in the streamwise direction in a manner that indicated wide variations of the flow coefficients for the individual perforations.

Nomenclature

a^* = speed of sound at sonic condition
D = diameter of perforation
H = δ^*/θ, shape factor
M = Mach number
p = pressure
u = streamwise velocity component
v = normal velocity component
w = mass flow rate
x = streamwise distance from shock-holder leading edge
y = distance from the top (interaction) wall
z = spanwise distance from model centerline
δ = boundary-layer thickness
δ^* = displacement thickness
θ = momentum thickness
ρ = density
σ = $-\rho_w v_w/(\rho_e u_e)_0$, local suction rate (normalized)
ϕ = flow coefficient for individual perforation

Subscripts

$b1$ = upstream end of the bleed zone
$b2$ = downstream end of the bleed zone
e = boundary-layer edge
t = stagnation (total) condition
p = plenum condition for the main channel flow
w = at the top wall
0 = located at the upstream reference station ($x = -44.4$ mm)

Superscript

$'$ = turbulent fluctuating component

Introduction

FLOWFIELDS in inlets of transonic and supersonic air-breathing propulsion systems are dominated by normal-shock/turbulent-boundary-layer interactions (NSTBLI). These interactions can substantially increase the boundary-layer thicknesses and turbulence intensities at the downstream end of the inlet (static distortion) and can also lead to large-scale, low-frequency fluctuations involving the entire flow (dynamic distortion). The resulting performance degradation becomes severe if the shock strength is sufficient to cause a shock-induced separation at the interaction, which generally occurs if the approach Mach number is greater than approximately 1.3.[1]

Shock/boundary-layer interactions may be divided into two major categories: supersonic interactions involving weak oblique shocks, where the post-shock flow is supersonic, and transonic interactions involving normal (or strong oblique) shocks, where the post-shock flow is subsonic.[1] Transonic interactions are strongly coupled to the entire subsonic field following the shock and in many respects behave quite differently than the more localized supersonic interactions.

The most common technique used to control either type of interaction is the removal of low-energy boundary-layer fluid through perforated or porous surfaces located in the interaction region, commonly called "bleed" in propulsion engineering.

A number of experiments involving mass removal from supersonic interactions have been performed and are discussed in reviews by Delery[2] and Hamed and Shang.[3] In contrast, there appears to be only one transonic interaction experiment involving mass removal in which velocity field data were obtained, performed by Chanetz and Pot.[4] They explored an airfoil-like flowfield with and without a passive control device that created a recirculation of air from behind the shock to upstream of the shock through a porous plate mounted over a cavity. This work appears to be the first laser-Doppler velocimetry (LDV) exploration of an interaction flowfield with mass removal. The mass flow involved in the recirculation could not be determined and the data are not directly applicable to the active mass removal devices typically used in inlets.

There are a number of investigations of entire inlets incorporating bleed systems,[3] the work of Wong[5] being perhaps most quoted. Since the emphasis in this category of contributions tends to be on the overall performance of the inlet, these papers generally offer only a limited amount of information on the interaction itself.

An overwhelmingly large fraction of the shock/boundary-layer interaction literature deals with solid-wall, unbled interactions. On the other hand, bleed systems are incorporated

Received Aug. 28, 1990; revision received May, 22, 1991; accepted for publication June 17, 1991.

*Scientist. Member AIAA.
†McDonnell Douglas Fellow. Associate Fellow AIAA.
‡Section Chief, Laboratory. Member AIAA.

in virtually all supersonic inlets, demonstrating that mass removal can substantially modify interactions in a wide range of applications. The result is that most of the available interaction literature has only an indirect, limited relevance to inlet technology.

The present paper contributes to filling this gap by exploring the consequences of imposing mass removal on a NSTBLI in which the shock strength, the post-shock channel geometry, and the ratio of the approach boundary-layer thickness to the channel height are representative of terminal shocks in supersonic inlets. Conditions are simplified by using a flat surface, a uniform approach flow, a number of channel configuration features intended to encourage two-dimensionality, and a perforation length scale that is significantly smaller than the boundary-layer thickness. The emphasis is on exploring the physical features introduced by the application of bleed, through a detailed, quantitative exploration of the entire flowfield.

The approach Mach number is 1.48 and the displacement thickness of the approach boundary layer is a relatively high 1.4% of the approach channel height. Detailed data were obtained both with and without mass removal from the boundary layer. The removed mass flow represented 97% of the displacement mass flow [defined as $(\rho_e u_e \delta^*)_0$] in the boundary layer approaching the interaction. Diagnostic techniques included flow visualization, time-mean wall-pressure measurements, and two-component LDV. The present paper describes the time-mean velocity field; turbulence properties have been determined also and are reported in Ref. 6.

Apparatus

The apparatus used in the present work was developed specifically for the study of shock/boundary-layer interactions (Fig. 1) and has been previously used to investigate an unseparated interaction at an approach Mach number of 1.34.[7] For the present work, the apparatus was modified to generate a uniform approach flow at $M = 1.48$. Detailed descriptions of the apparatus are included in Refs. 7 and 8; only a brief version can be given here.

A uniform supersonic flow was generated by a symmetric, two-dimensional, supersonic nozzle. The boundary layer was allowed to grow on the flat top wall, but the side- and bottom-wall boundary layers were removed through upstream-facing slots. This arrangement resulted in a thick top-wall boundary layer that accounted for approximately 63% of the total displacement area at the nominal location of the normal shock. The large blockage fraction represented by the top-wall boundary layer is expected to cause the top layer to dominate the interaction.

The shock could be positioned by a flap-type throttling device located at the downstream end of the model. The leading edge of the bottom-wall slot acted as shock holder, stabilizing the bottom end of the normal shock. The flow exhausted to the atmosphere after the throttle. The sidewalls of the model held two pairs of glass windows for optical access to most of the flowfield. A schematic diagram of the shock holder and the nearby duct features are presented in Fig. 2.

The top wall incorporated a full-span, removable panel that allowed the use of any type of wall surface over a 311-mm streamwise length. For the no-bleed case this panel held a smooth, solid wall. For the bleed case, the panel incorporated a full-span strip of finely perforated plate ($D/\delta_0^* \cong 0.02$), with 7% open-area fraction (Fig. 2). The downstream edge of the perforated strip was located at $x = 0$, such that the flow was supersonic over the bleed zone. Uniform back pressure was maintained on the outside of the perforated strip by covering it with a large vacuum plenum chamber (VPC, Fig. 1) and connecting the chamber to a high-capacity vacuum pump.

Diagnostic Methods

A variety of diagnostic techniques were used, as described in detail in Refs. 7 and 8; only a brief description can be given here. Wall static-pressure distributions were determined by

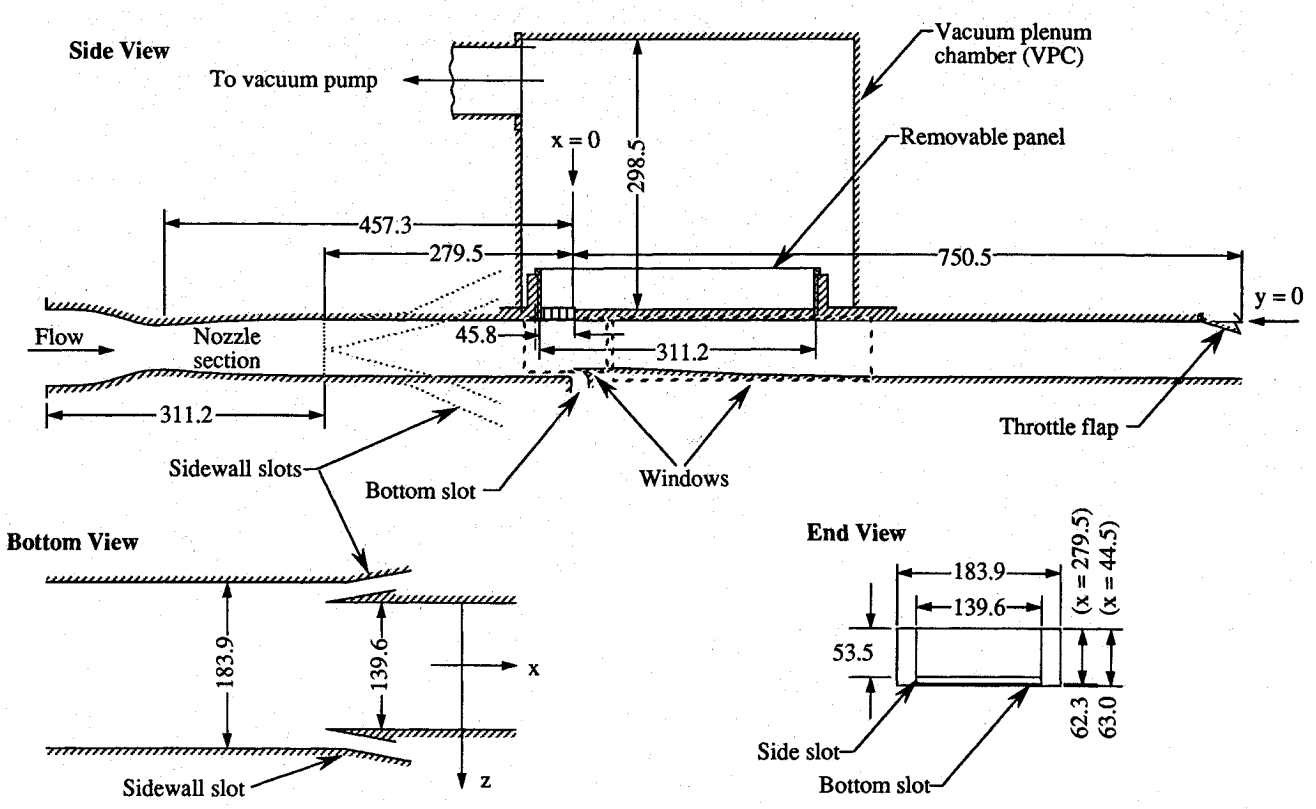

Fig. 1 Experimental apparatus for the study of shock/boundary-layer interaction with mass removal. Removable top panel accepts perforated segments of arbitrary configuration.

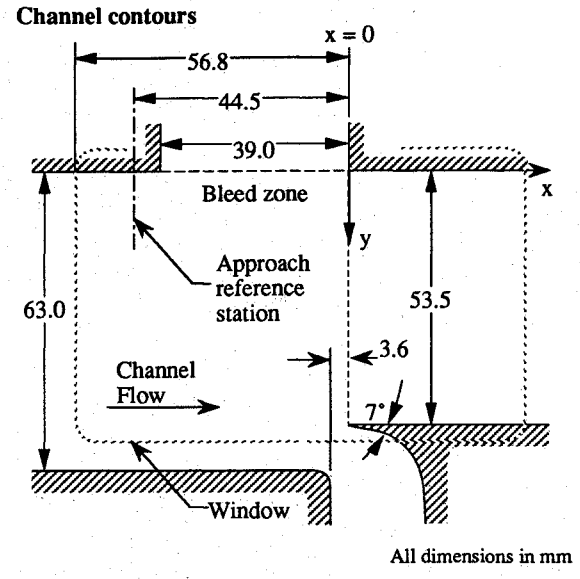

Fig. 2 Details of test section for the bleed flow case.

means of numerous static-pressure taps. High-speed schlieren movies, spark schlieren photographs, and a video camera coupled to a synchronized strobe light provided visual information, and a surface oil-flow technique was used to determine qualitative wall-shear patterns.

The two-component laser-Doppler velocimeter used a 5-W argon-ion laser and operated in the forward scatter mode. The velocity vector field was obtained in the plane of symmetry both with and without suction. Data were obtained at 24 or more streamwise stations and at 30 or more vertical locations at each station. Velocity measurements were also made over three complete cross sections to determine the evolution of three-dimensional features. The data extended from the inviscid core flow to within 0.25 mm of the wall. In the mass removal case, 18 additional stations were used to improve resolution over the perforated surface. Samples of 5000 bursts (coincident within 1 μs) were used at each measurement point.

Operating Conditions

The approach stagnation pressure was 240 kPa. The stagnation temperature of the air varied with ambient conditions, giving rise to a $\pm 5\%$ variation of Reynolds number. Since Reynolds number dependence is weak, this variation was not considered significant. The approach boundary layer on the top wall was turbulent: transition occurred naturally, probably upstream of the nozzle throat.

The velocity profile at the upstream reference station ($x = -44.5$ mm, $z = 0$) was, for unbled flow, an essentially fully developed, zero pressure gradient turbulent boundary layer ($\delta_0 = 7.3$ mm, $\delta_0^* = 1.08$ mm, $\theta_0 = 0.47$ mm, $\Pi_0 = 0.5$, $Re_{\theta 0} = 14{,}000$, details in Ref. 8). In the bleed case, the upstream influence of the bleed zone was greater than expected and the velocity profile at the same station was somewhat different ($\delta_0 = 5.9$ mm, $\delta_0^* = 1.07$ mm, $\theta_0 = 0.41$ mm, $\Pi_0 = 0.8$, $Re_{\theta 0} = 12{,}000$, details in Ref. 8). Further upstream, outside the optically accessible region, the boundary layers are believed to be identical for both cases, having been generated by the same approach channel (no disassembly of the approach sections took place between the two series of tests).

The total mass flow removed through the perforated plate (per unit span) was determined by integrating the centerline $(\rho v)_w$ distribution over the perforated surface. The density was estimated using the measured wall static pressure and by assuming the total temperature to be that of the freestream.

Preliminary Experiments

Several exploratory tests were performed to determine an appropriate streamwise location for the perforated region (bleed zone) relative to the shock. Tests were run with 1) bleed zone leading edge at the shock ($x_{b1} = 0$), 2) the center of the zone at the shock ($x_{b1} = -19.5$ mm), and 3) the trailing edge of the zone at the shock ($x_{b1} = -39.0$ mm).

Visual observation and videotapes clearly showed that cases 1 and 2 led to strong distortions: the bottom end of the shock remained attached to the shock holder while the top end moved to the downstream edge of the bleed zone, creating an oblique, curved shock. In case 1 the shock was oscillating randomly with a large amplitude (approximately 25 mm peak-to-peak) for reasons not understood. The large-amplitude oscillation left little hope of obtaining meaningful LDV data in the region swept out by the shock for cases 1 and 2.

The supersonic bleed (case 3) is least favored for applications because it requires a much lower back pressure than does a subsonic bleed and because it disturbs the freestream approaching the interaction. However, this configuration led to a relatively simple wave pattern, a nearly normal shock, and was significantly more stable than the other two cases, which justified its selection for detailed LDV measurements.

The effect of varying the VPC pressure level was studied briefly for case 3. When the VPC pressure reached an intermediate value between the pre- and post-shock pressures, an oblique shock wave appeared anchored to the leading edge of the bleed zone. This condition was interpreted to indicate the presence of "blowback," i.e., entry of air from the VPC into the supersonic mainstream. The flow also became more unsteady with shock oscillations of significantly larger amplitude. These phenomena are undesirable and were avoided throughout the tests by always keeping the VPC pressure sufficiently low to ensure the choking of all perforations.

Overall Features of the Flows

The spark schlieren photos and qualitative sketches in Figs. 3 and 4 illustrate the main features of the flows. The no-bleed flow (Fig. 3) displayed the lambda pattern typically associated with a shock-induced separation. The presence of separation was confirmed both by LDV data and by oil-flow visualization of the shear stress patterns on the top wall. The rapid growth of the boundary layer is evident from the photograph. The top- and bottom-wall boundary layers met and terminated the inviscid core flow at $x \cong 130$ mm. High-speed schlieren movies indicated that the interaction was relatively steady: the upstream leg of the shock at the wall displayed a streamwise jitter of approximately ± 2 mm amplitude.

The flow with bleed presented an entirely different pattern (Fig. 4). An expansion fan originated near the beginning of

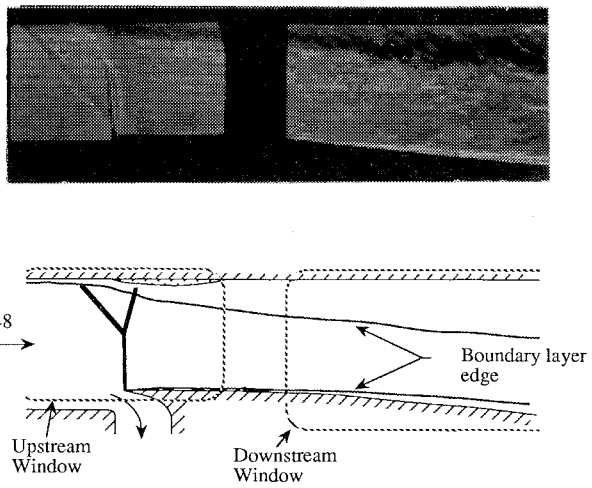

Fig. 3 Features of the shock/boundary-layer interaction with no bleed.

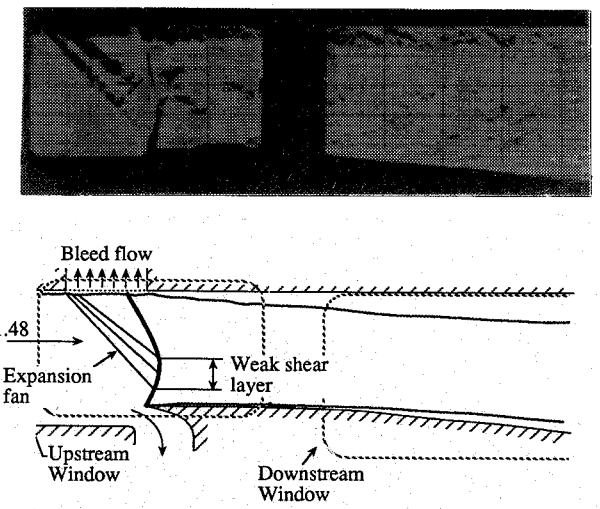

Fig. 4 Features of the shock/boundary-layer interaction with bleed.

the bleed zone, deflecting the supersonic flow towards the wall. The shock was a single line (no bifurcation), intersecting the top wall at $x \cong -5$ mm, upstream of the end of the bleed zone, while the bottom end was attached to the shock holder. The expansion fan intersected with and deformed the shock wave approximately 30 to 35 mm from the top wall. The schlieren images and plane-of-symmetry LDV measurements both indicated unseparated flow throughout. High-speed schlieren movies showed increased unsteadiness: the upstream leg of the shock at the wall oscillated with an amplitude of approximately ± 4 mm.

Wall Pressure Distributions

Streamwise pressure distributions for the no-bleed and bleed cases are compared in Fig. 5. The no-bleed case shows the gradual pressure rise typical of separated NSTBL interactions. The case with bleed shows a more complex behavior: a sharp minimum exists at the beginning of the bleed zone, followed by a comparably sharp local maximum near the zone end. The minimum is associated with the local acceleration around the upstream corner as the bleed flow executes a 90-deg upward turn. The same feature has been observed in low-speed flow into an open slot normal to the wall[9] (without a perforated plate); apparently the presence of the plate only modifies but does not eliminate the minimum. The pressure maximum reflects the proximity of the stagnation point that terminates the streamline separating the bleed stream from the main flow near the downstream corner.

The pressure rise between the two extrema is much steeper in the bleed case: the removal of the boundary layer allows the imprint of the shock pressure jump on the wall much more closely. As will be shown later, this steepness has an adverse effect on the sidewall boundary layers.

The wall pressure at the end of the channel reaches significantly higher levels in the bleed flow: the highest pressure ratio achieved changes from 0.70 to 0.74. The increase is explained by the reduction of the core velocity at the exit station, due in part to removing approximately 0.6% of the mass flow through the bleed system and in part to the larger effective area at the exit, created by the reduced boundary-layer displacement thickness.

Spanwise Variations

Velocity distributions were determined over most of the cross-sectional area at three streamwise stations: before the shock, shortly after the shock, and at the end of the divergent section. The results (Figs. 6 and 7) show that the flow approximated two-dimensional behavior surprisingly well for the no-bleed case, but not for the case with bleed. Mass removal caused unequal growth rates of the sidewall boundary layers in the subsonic region, leading to an asymmetric channel flow at the subsonic measurement stations. The observed rapid growth rate on the sidewall is probably indicative of separation; evidence of reversed flow was seen in LDV data approximately 6 mm from the sidewall. The flow selected the $+z$ sidewall for rapid growth, probably due to some small initial asymmetry in the approach flow. The supersonic flow was very nearly two-dimensional in both cases.

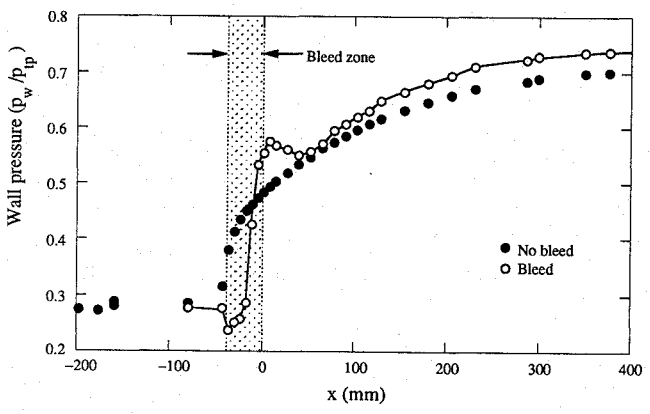

Fig. 5 Top-wall pressure distributions with and without bleed.

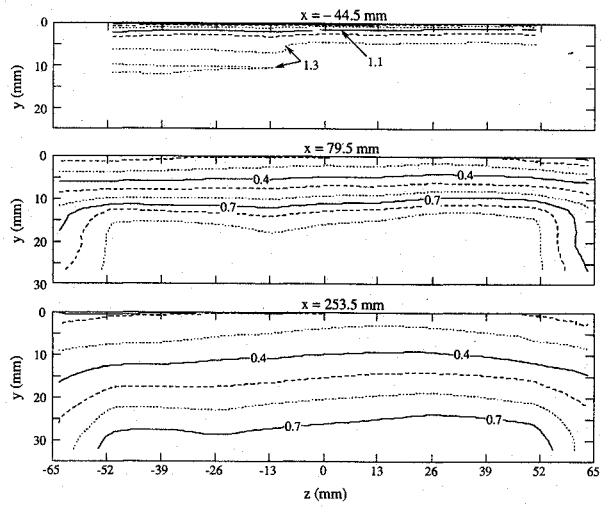

Fig. 6 Evolution of three-dimensional features of flow with no bleed. Contours show constant values of u/a^* in three cross-sectional planes.

In a separate test the front window pair was replaced with sidewalls incorporating bleed zones having the same streamwise extent and porosity as those on the top wall. Pressure rake data obtained at $x = 79.5$ mm, at three different spanwise locations ($z = 0, \pm 35$ mm), resulted in essentially identical profiles, indicating a symmetric flow at this station. Sidewall bleed thus appears to cure the asymmetry; unfortunately the possibility of obtaining LDV data is also lost.

Velocity Field in the Plane of Symmetry

Contour maps of u/a^* are used to illustrate the overall appearance of the two flowfields. The no-bleed case (Fig. 8a) displays a shock-induced separation and the associated lambda pattern (clear on schlieren photos, imperfectly represented on the contour plot). The divergent contours along the top wall describe a rapidly growing top-wall boundary layer. The Mach number is very close to unity in a fairly large-core flow region downstream of the shock. The separated-flow region is characterized further in Fig. 9, using contours of the probability of occurrence of negative u. The highest value, 55%, was measured at locations nearest to the wall, corresponding to an "incipient detachment" in the terminology of Ref. 10. Interestingly, the measured mean velocity at the same location was positive, an apparent paradox made possible by the skewness of the LDV histograms. Oil flows showed a distinct separation line at $x = -10$ mm, but a definite reattachment location could not be identified in the patterns.

Figure 8b illustrates the bleed case. The apparent entry of some contours into the wall over the bleed zone reflects the thinning of the boundary layer by the mass removal, and the closely clustered contours along the subsonic portion of the top wall likewise correspond to a top-wall boundary layer that is much thinner than its no-bleed counterpart. The expansion fan initiated by the leading edge of the bleed zone is evident.

Velocity profiles for the no-bleed case (Fig. 10) show the variations expected of a separated NSTBLI on the basis of numerous earlier studies.[1] The corresponding profiles for the bleed case (Fig. 11) begin with a slightly thinner boundary layer at $x = -44.5$ mm, due to the upstream influence of the suction, as mentioned earlier. Profiles over the bleed zone show the effects of the expansion fan in the form of an outward moving, higher-than-freestream velocity region. Apart from the expansion fan, the viscous layer thickness remains more or less constant over the bleed zone; the mass removal is

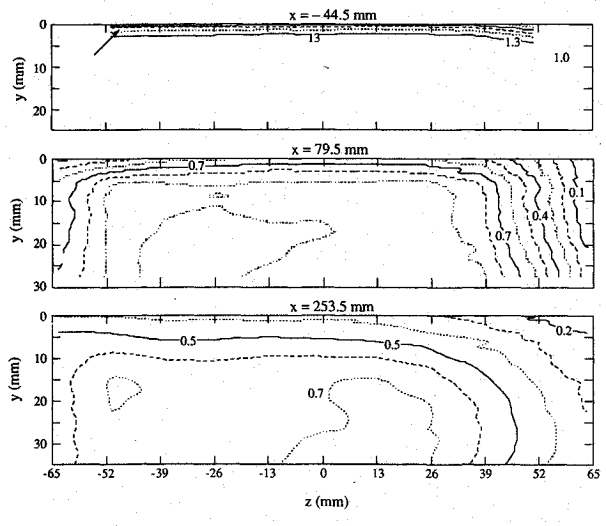

Fig. 7 Evolution of three-dimensional features of flow with bleed. Contours show constant values of u/a^* in three cross-sectional planes.

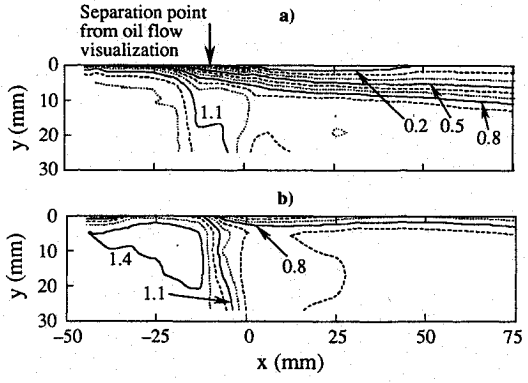

Fig. 8 Contours of u/a^*. a) No bleed; b) with bleed.

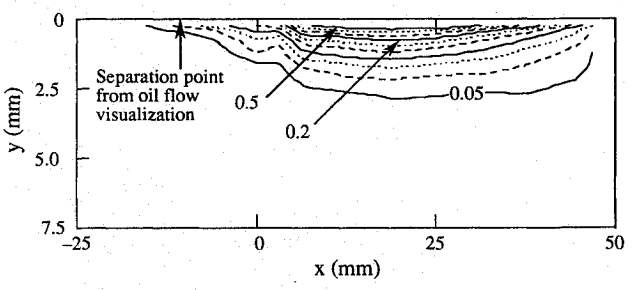

Fig. 9 Contour lines indicate fraction of time for which instantaneous x component of velocity is negative. Flow with no bleed. Note expanded vertical axis.

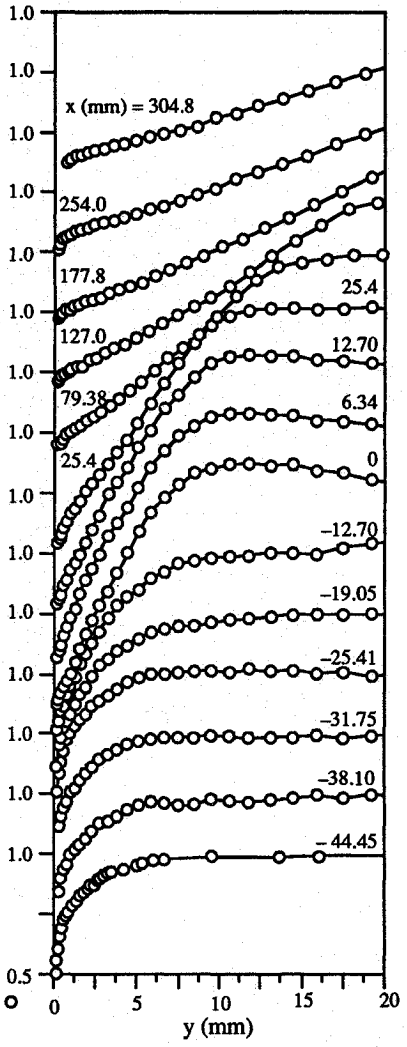

Fig. 10 Profiles of x component of velocity for the no-bleed flow, normalized by edge velocity. The lowest tic mark labeled 1.0 on the vertical axis is assigned to $x = -44.5$ mm. Profiles for other x positions are shifted successively upward, each by 0.25.

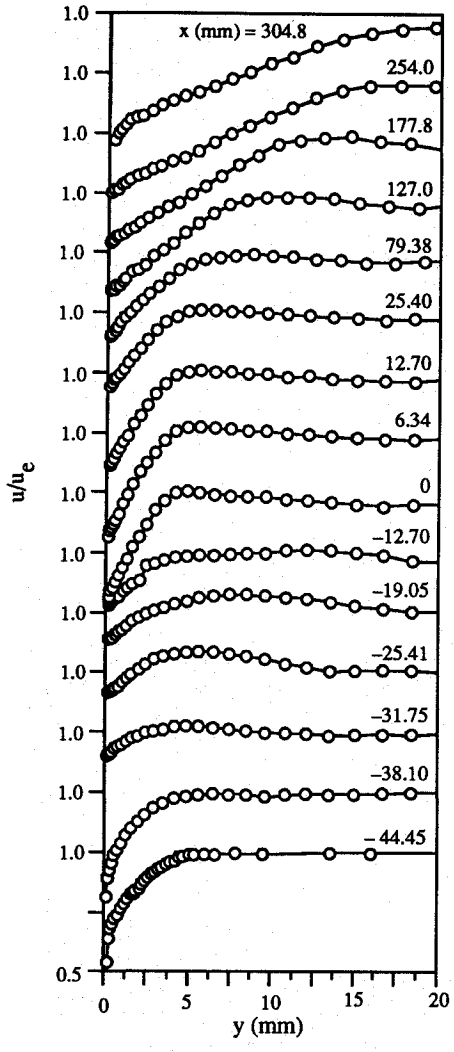

Fig. 11 Profiles of x component of velocity for the bleed flow, normalized by edge velocity. The lowest tic mark labeled 1.0 on the vertical axis is assigned to $x = -44.5$ mm. Profiles for other x positions are shifted successively upward, each by 0.25.

nearly balanced by the entrainment. The velocity profiles are much fuller everywhere, and there is no evidence of reversed flow at any location.

Normal velocity components (v) were determined throughout and have been published in Ref. 8. Conditions over the bleed zone are illustrated in Fig. 12, using an expanded x scale. The wall static pressure rises rapidly within the zone, and, since the flow through the wall perforations is choked, one would expect a similar distribution for the normal velocity at the wall. The actual trend, however, is very different: v reaches an early peak, only to decline sharply to much lower values over the rest of the bleed zone. Normal velocity distributions [$v(x)$] were obtained at several distances from the wall: for $y < 3$ mm the distributions are quite insensitive to y, implying that extrapolation of $v(y)$ to the wall is a valid method to determine v_w. The local bleed mass flow (σ, also shown) was calculated using densities based on the measured static pressure and assuming the total temperature to be the same as the freestream value.

It is noted that the results in Fig. 12 refer to supersonic flow and are not affected by the asymmetry of the subsonic sidewall boundary layers.

Boundary-Layer Development

The streamwise distributions of top-wall boundary-layer parameters are given in Figs. 13–16 for both flows. The parameters were calculated using the conventional definitions for compressible boundary layers. Density was determined from the measured wall static pressure and assuming the total temperature to be equal to that of the freestream. The somewhat subjective determination of the boundary-layer edge location was aided by considering the u' rms profiles, which displayed relatively well-defined features at the edge.

The no-bleed boundary layer grows monotonically, without displaying the displacement-thickness maxima observed in most past studies (Ref. 11). The gradual nature of the growth found here suggests that the separated-flow region is substantially thinner in this case than those discussed in Ref. 11. As suggested in Ref. 8, the relatively high upstream blockage in this experiment may play a role in this apparent attenuation of separation.

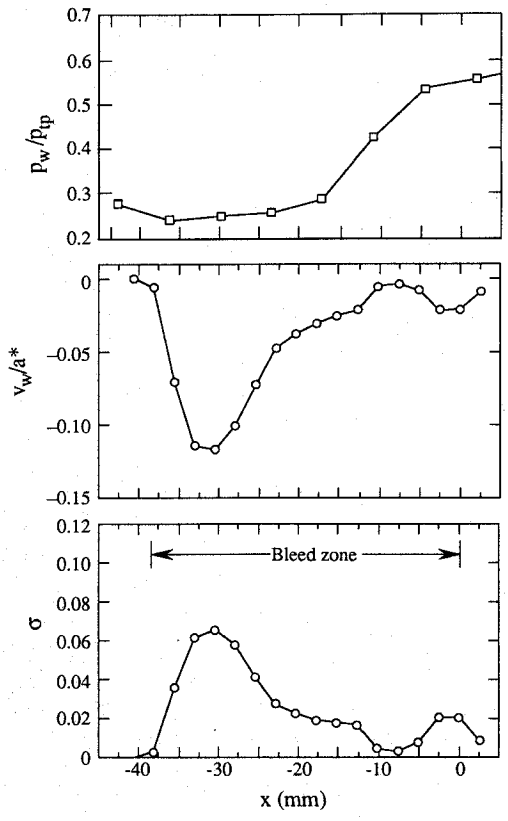

Fig. 12 Flow property distribution in bleed zone. From top to bottom: wall static pressure, vertical velocity component, normalized mass flow. Velocities measured at $y = 0.25$ mm.

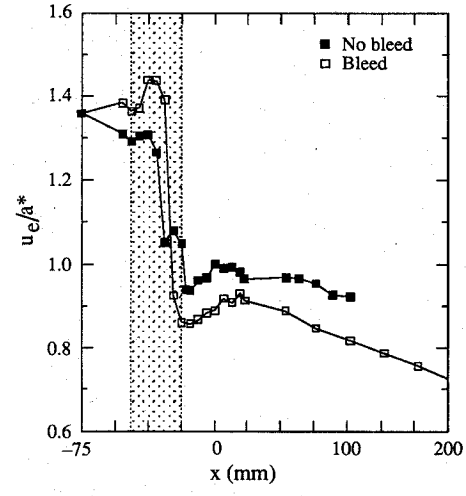

Fig. 13 Boundary-layer edge velocity with and without bleed.

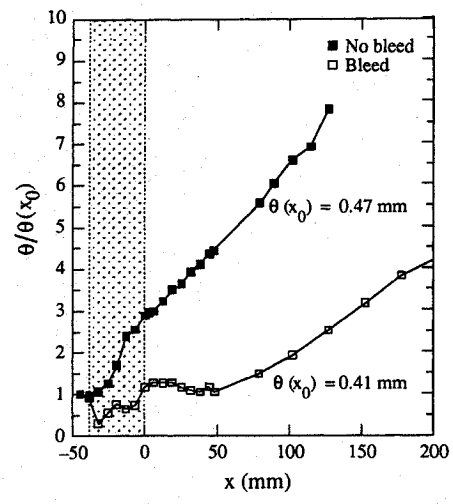

Fig. 14 Boundary-layer momentum thickness distributions with and without bleed.

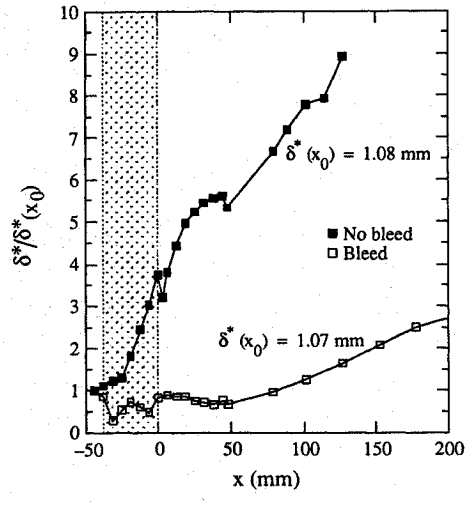

Fig. 15 Boundary-layer displacement thickness distributions with and without bleed.

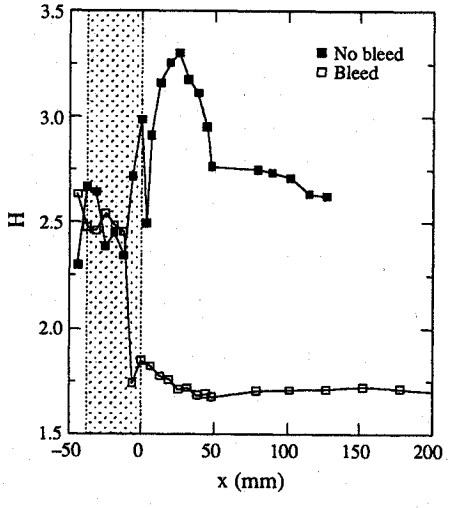

Fig. 16 Boundary-layer shape factor distributions with and without bleed.

Mass removal keeps the boundary-layer thicknesses more or less unchanged across the bleed zone. The boundary-layer thicknesses are decreasing in the x range from 10 mm to 50 mm, as also noticeable in the contour plot of Fig. 8b. The reason is not understood. Further downstream the normalized boundary-layer thicknesses are only one-half to one-third of those for the no-bleed case. In particular, the momentum thickness at $x = 130$ mm is reduced by bleed to one-third of the values observed in the no-bleed case (Fig. 14). The displacement thickness (Fig. 15) was reduced by a factor of six at the same location, which must be a factor in elevating the static pressure at the channel end (Fig. 5). The shape factor distributions shown in Fig. 16 are also instructive: the high values found for the no-bleed case are consistent with the occurrence of separation, and the very low values created by suction are consistent with the low rates of growth found downstream of the bleed zone.

Discussion

In this section speculative comments are offered on the possible reasons for some of the unexpected findings. One issue concerns the unexpected streamwise distribution of the bleed mass flow. If the flow coefficients[§] ϕ were the same for all perforations, then the σ distribution would be very similar to that of the wall static-pressure distribution. Mostly for want of any relevant information, ϕ is often assumed to be constant in design and/or in computational prediction of bleed flows. Figure 12 demonstrates that this assumption is not admissible: the flow coefficient must vary between wide limits to account for the variation of ϕ actually observed. It is reasonable to expect that ϕ would be dependent on the conditions immediately preceding the hole in question, including the pressure ratio across the hole, the ratio of the hole diameter and the boundary-layer thickness, the freestream Mach number, and several other factors. Figure 12 suggests that such dependencies not only exist but are strong.

A possible explanation for the large variation of the flow coefficient is as follows. Initially the holes "see" a reasonably thick viscous sublayer and sonic layer (the hole diameter, normalized by the viscous sublayer scale, is 58). The thicknesses of both layers approaching a given hole are reduced by suction through all upstream-lying holes, leaving virtually no viscous sublayer and virtually no subsonic flow. Under these conditions the flow is locally supersonic and must be deflected into the hole through an expansion fan. The attainable deflection is limited by the pressure existing in the VPC (to approximately 13 deg in this case). Inviscid analyses show that this mechanism can reduce the flow coefficient by an order of magnitude.[12]

This finding suggests that the numerical prediction of bleed flows must be based either on resolving the flow details on the scale of the individual perforations, or on detailed empirical information concerning the dependence of the flow coefficients on the properties of the local flows approaching each perforation (as affected by all other upstream perforations).

A second unexpected finding is the substantially increased unsteadiness of the shock, caused by placing part or all of the bleed zone in a nominally subsonic region. The existence of such fluctuations is contrary to the intuitive but common notion that suction generally exerts a stabilizing influence on NSTBLIs. The shock appeared to be most stable when attached to the downstream end of the bleed zone.

[§]The flow coefficient for an individual perforation ϕ is defined according to accepted practice (Ref. 12), as the actual mass flow through the hole, divided by the mass flow that would pass through the same hole if 1) the fluid was inviscid, 2) the flow had a total pressure equal to the wall static pressure, 3) the fluid had a total temperature equal to that of the freestream, and 4) the back pressure was sufficiently low for the flow to be choked.

The third comment relates to the sidewall separation caused by the bleed. As described in the "Introduction," the configuration design was oriented towards creating a nearly two-dimensional flow. The actual geometry was as symmetric as careful machining and assembly can allow and a detailed exploration of the velocity distributions entering the nozzle found no asymmetries beyond the tolerance of the measurements.

In view of the substantial effort expended in this direction, the inability to achieve a nearly two-dimensional subsonic flow in the bleed case is disappointing, but also meaningful. It appears that the bleed flow investigated here has an extreme tendency to translate a minor upstream asymmetry into a major one downstream of the interaction. Such tendencies have been found in other flows, e.g., two-dimensional diffusers prone to bistable behavior and slender body flows at high angles of attack, where grossly asymmetric vortex shedding can occur.

The mechanism by which the asymmetry is amplified probably involves a bleed-induced steepening of pressure jumps on the sidewalls. The unbled sidewall boundary layers are unable to negotiate the rapid rise and rapid thickening and/or separation results. From the application point of view, it follows that a bleed system covering the entire circumference should perform better than one that confines bleed to only part of the perimeter.

Summary

Mass removal through a perforated plate from a boundary layer approaching a NSTBL interaction created an entirely different and considerably more complex flowfield than the unmodified flow. Mass removal generated an expansion fan at the leading edge of the bleed zone that interacted with and modified both the approaching flowfield and the normal shock. Boundary-layer separation from the interaction wall was eliminated. The thickness and the rate of growth of the post-shock boundary layer was greatly reduced and ultimately the mass removal resulted in improved recovery of static pressure in the duct.

The streamwise distribution of the mass flow over the perforated surface displayed strong variations, explained by large variations of flow coefficients for individual perforations.

Mass removal accelerated development of three-dimensional features downstream of the shock and led to asymmetric sidewall boundary-layer growth. The commonly observed unsteadiness of NSTBL interactions was greatly increased if the bleed zone extended even partially downstream of the position occupied by the shock in the unbled flow.

This investigation has revealed the complexity of the flow in one particular bleed system configuration. The acquisition of information needed to optimize bleed systems would require extensive investigations of the numerous parameters required to define a system. The large number of parameters precludes completeness, but some reasonable exploration of the indicated dependencies is highly desirable.

Acknowledgment

This research was conducted under the McDonnell Douglas Independent Research and Development program.

References

[1]Delery, J., and Marvin, J. G. (eds.), "Shock Wave Boundary Layer Interactions," AGARD Rept. AG-280, Feb. 1986.

[2]Delery, J., "Shock-Wave/Turbulent Boundary-Layer Interaction and its Control," *Progress in Aerospace Sciences*, Vol. 22, 1985, pp. 209–280.

[3]Hamed, A., and Shang, J., "Survey and Assessment of Validation Data Base for Shockwave Boundary Layer Interactions in Supersonic Inlets," AIAA Paper 89–2939, July 1989.

[4]Chanetz, B., and Pot, T., "Fundamental Experiments on the Passive Control of Shockwave/Boundary Layer Interaction in the Supersonic Region," ONERA Rept. TP 1987–183, Oct. 1987.

[5]Wong, W. F., "The Application of Boundary Layer Suction to Suppress Strong Shock-Induced Separation in Supersonic Inlets," AIAA Paper 74–1063, Oct. 1974.

[6]Morris, M. J., and Sajben, M., "The Effects of Mass Removal on the Turbulent Properties of a Normal-Shock/Turbulent-Boundary-Layer Interaction," AIAA Paper 91–0647, Jan. 1991.

[7]Sajben, M., Morris, M. J., Bogart, T. J., and Kroutil, J. C., "Confined Normal-Shock/Turbulent-Boundary-Layer Interaction Followed by an Adverse Pressure Gradient," AIAA Paper 89–0345, Jan. 1989.

[8]Morris, M. J., Sajben, M., and Kroutil, J. C., "Experimental Investigation of Normal-Shock/Turbulent-Boundary-Layer Interactions with and Without Mass Removal," AIAA Paper 90–0379, Jan. 1990.

[9]Khan, M. M. S., Cornelius, K. C., and Tassa, Y., "Effect of Suction on Boundary-Layer Flow Over a 2–D Slot," AIAA Paper 82–0222, Jan. 1982.

[10]Kline, S. J., Barolina, J. G., and Strawn, R. C., "Correlation of the Detachment of Two-Dimensional Turbulent Boundary Layers," *AIAA Journal*, Vol. 21, No. 1, 1982, pp. 68–73.

[11]Schofield, W. H., "Interaction of a Turbulent Boundary Layer with a Normal Shock Wave Followed by an Adverse Pressure Gradient," Aeronautical Research Laboratories, Melbourne, Victoria, Rept. AR-002–950, April 1983.

[12]Haas, M., and Karanian, A. J., "Bleed-Bypass Concepts for Supersonic Inlets," Naval Weapon Center Rept., NWC TP 6379, Aug. 1983 (unclassified).